Title
DIFFRACTION DISSOCIATION IN 205 GeV/c n-p TWO-AND FOUR-PRONG INTERACTIONS

Authors
Abrams, G.S.
Bingham, H.H.
Chew, D.M.
et al.

Publication Date
1973-08-10

Presented at the APS Division of
Particle and Fields Meeting,
Berkeley, CA, Aug. 13-17, 1973

LBL-2112

c.1

DIFFRACTION DISSOCIATION IN 205 GeV/c π^-p TWO- AND FOUR-PRONG INTERACTIONS

G. S. Abrams, H. H. Bingham, D. M. Chew,
B. Y. Daugéras, W. B. Fretter, C. E. Friedberg,
G. Goldhaber, W. R. Graves, A. D. Johnson, J. A. Kadyk,
L. Stutte, G. H. Trilling, F. C. Winkelmann, G. P. Yost
D. Bogert, R. Hanft, F. R. Huson, D. Ljung,
C. Pascaud, S. Pruss, W. M. Smart

August 10, 1973

Prepared for the U. S. Atomic Energy Commission
under Contract W-7405-ENG-48

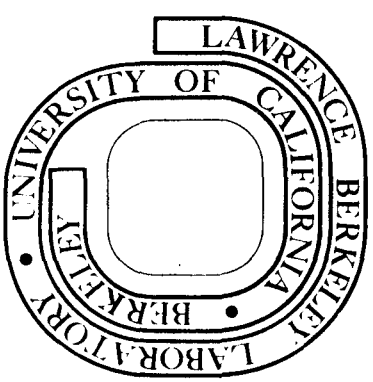

LBL-2112

DISCLAIMER

LBL-2112

DIFFRACTION DISSOCIATION IN 205 GeV/c π^-p TWO- AND FOUR-PRONG INTERACTIONS*

G. S. Abrams, H. H. Bingham, D. M. Chew, B. Y. Daugéras,†
W. B. Fretter, C. E. Friedberg, G. Goldhaber, W. R. Graves,
A. D. Johnson, J. A. Kadyk, L. Stutte, G. H. Trilling,
F. C. Winkelmann and G. P. Yost

Department of Physics and Lawrence Berkeley Laboratory
University of California, Berkeley, California 94720

and

D. Bogert, R. Hanft, F. R. Huson, D. Ljung,
C. Pascaud,† S. Pruss, W. M. Smart

National Accelerator Laboratory
Batavia, Illinois 60510

August 10, 1973

I. INTRODUCTION

We present data on diffraction dissociation in 2- and 4-prong channels produced by 205 GeV/c π^-p interactions in the NAL 30-inch hydrogen bubble chamber. The unseparated 205 GeV/c negative particle beam was produced by targeting 303 GeV/c protons from the NAL Synchrotron and was transported one km to the bubble chamber. Beam characteristics at the chamber were as follows: a momentum spread of ±0.1%, an angular divergence of ±0.25 mrad, and K^-, $\bar{p}$ and μ^- contaminations of 1.4±0.2%, 0.16±0.1% and 2.2±0.03%, respectively. The data presented here are based on almost the complete data sample in an exposure of 48K pictures with an average of 7 beam tracks/frame. The film was scanned with approximately lifesize projection in 3 separate views, by physicists and independently by professional scanners. Discrepancies were resolved using a scan table projecting 3.5X lifesize images. The events accepted in the scan were restricted to a fiducial volume approximately 40 cm long in the beam direction. A more restrictive fiducial volume (omitting

the last 11 cm along the beam) was used in this analysis in order to insure more accurate reconstruction of fast forward tracks. The events were measured on film-plane measuring projectors. Bubble density patterns were compared in each view in order to ensure proper track matching. Geometrical and kinematic fitting were performed with the standard programs TVGP and SQUAW.

II. DISCUSSION OF CONSTRAINED FITS

The constrained fits considered in the analysis were the following,

$$\pi^- p \rightarrow \pi^- p \quad , \tag{1}$$

$$\pi^- p \rightarrow \pi^- \pi^- \pi^+ p \quad , \tag{2}$$

both nominally 4-constraint fits. Although elastic scattering [reaction (1)] is not discussed in this paper, the problem of separating inelastic from elastic two-prong events is relevant to our considerations. At intermediate energies ($P_{LAB} \lesssim 10$ GeV/c), the four-constraint fits are sufficiently powerful, particularly if coupled to bubble density information, to identify with very little ambiguity the real examples of reactions (1) and (2). At 205 GeV/c, however, momentum measurement uncertainties are such as to require further study of the validity of the fits and the magnitude of background included in them.

Such a study was carried out in the following manner. We computed directly from the measurements the following quantities:

(a) The mass squared, M_R^2, recoiling against the proton (2-prong events) or recoiling against the combination--proton plus two slowest pions (4-prong events). For the real examples of reactions (1) or (2), this quantity M_R^2 must, within the errors, agree with the mass squared of a pion, 0.019 GeV^2. The error width in M_R^2 is typically ± 1.5 GeV^2 and is largely determined by the uncertainty in the direction of the recoil proton.

(b) The total outgoing transverse momentum component $\Delta P_{T\varphi}$ in the plane perpendicular to the camera lens axis. To sharpen this quantity, we replace the momentum of the fastest outgoing pion [or the only outgoing pion for reaction (1)] by the value predicted from longitudinal momentum balance. Furthermore we use this modified momentum value to re-evaluate the direction of the pion at the interaction vertex, the significance of this arising from the fact that the main azimuthal uncertainty comes from the curvature uncertainty of the track. With this procedure, the typical error width of $\Delta P_{T\varphi}$ is ± 50 MeV/c. For real examples of (1) and (2), $\Delta P_{T\varphi}$ is of course predicted to be zero whereas for events which do not fit (1) and (2) we would usually expect values of several hundred MeV/c. It is necessary to note that $\Delta P_{T\varphi}$ as calculated here is not a valid quantitative measure of actual transverse momentum imbalance for events not fitting (1) or (2) since longitudinal momentum conservation is explicitly incorporated in the calculation. However it serves the needed purpose of a quantity which should be close to zero for a real fit and broadly distributed for the background.

The additional constraints of longitudinal momentum conservation and conservation of transverse momentum component in the direction of the camera lens axis involve quantities too imprecisely measured to provide sharp tests of fits to reactions (1) and (2).

Applying these considerations to reaction (1), we show in Fig. 1a a two-dimensional histogram of M_R^2 vs $\Delta P_{T\varphi}$ for 2-prong events and in Fig. 1b the corresponding histogram for those events which kinematically fit reaction (1) with a $\chi^2 < 30$. It is apparent that essentially all the real elastics have $|\Delta P_{T\varphi}| < 0.20$ GeV/c, and that with $|\Delta P_{T\varphi}| > 0.25$ GeV/c one has a sample of largely inelastic events. By examining the distributions of $\Delta P_{T\varphi}$ for "2-prong events" manufactured by throwing away two pions from measured 4-prong

events, we can determine the shape of the background and thereby estimate the fraction of inelastic events hiding under the elastic peak in Fig. 1, namely about 4% of the elastic events.

Coming now to reaction (2), we anticipate slightly our later discussion by noting that almost all events fall into the class of pion diffraction (three fast π and slow proton) or nucleon diffraction (single fast π^- and slow proton, slow π^+, slow π^-). Figure 2ab exhibit two-dimensional histograms of M_R^2 vs $\Delta P_{T\varphi}$ for pion diffractions and Fig. 3ab exhibit similar histograms for the nucleon diffraction events. The background under the 4C fits is about 25% (10%) for the pion diffraction (nucleon diffraction) events. This background can be reduced considerably by appropriate cuts as discussed further.

An important qualification must be added to the above discussion. For pion diffraction events, we have essentially no way of distinguishing reaction (2) from the following,

$$\pi^- p \rightarrow \pi^- K^- K^+ p \quad . \tag{3}$$

Thus, although in our subsequent analysis we shall neglect (3) we must recognize that whenever dissociation of the form ($\pi^- \rightarrow \pi^-\pi^-\pi^+$) or ($\pi^- \rightarrow \pi^-\pi^-\pi^+ +$ neutrals) is discussed it includes contributions of the type ($\pi^- \rightarrow \pi^- K^- K^+$) and ($\pi^- \rightarrow \pi^- K^- K^+ +$ neutrals).

III. THE REACTION $\pi^- p \rightarrow \pi^-\pi^-\pi^+ p$

From study of Figs. 2a and 3a and subtraction of the background, we find a cross section for the reaction (2) of 530±65 μb.[1] The momentum dependence of this cross section is shown in Fig. 4.[2] It clearly appears to be dropping only slowly between 20 and 205 GeV/c, indicative that diffractive processes may be playing a dominant role.

Our subsequent discussion of this process is based on 128 fitted events

within our rather restricted fiducial volume (which provides at least 26 cm of path length for the measurement of fast forward tracks). These events contain backgrounds as discussed above of 25% (pion diffraction) and 10% (nucleon diffraction); and, in some of our histograms, we reduce the relative pion diffraction background population by about a factor of 2 by additionally requiring that $|\Delta P_{T\varphi}| < 0.1$ GeV/c (see Fig. 2).

In Fig. 5, we show a two-dimensional histogram of the $\pi^-\pi^-\pi^+$ mass vs the lower of the two possible $p\pi^+\pi^-$ masses. The striking features of this plot are:

(i) A clear grouping of low (< 3.2 GeV) $p\pi^+\pi^-$ mass events, presumably involving nucleon diffraction,

$$\pi^- p \rightarrow \pi^- (\pi^-\pi^+ p) \quad .$$

(ii) Another clear grouping of low (< 3 GeV) $\pi^-\pi^-\pi^+$ mass events, presumably involving pion diffraction,

$$\pi^- p \rightarrow (\pi^-\pi^-\pi^+) p \quad .$$

(iii) Finally a few events which exhibit fairly high $p\pi^+\pi^-$ and $\pi^-\pi^-\pi^+$ masses and perhaps do not belong in the two above categories. As discussed elsewhere these may be interpreted in terms of double-Pomeron exchange processes.[3]

Figures 6ab and 7ab show the $\pi^-\pi^-\pi^+$ and $p\pi^+\pi^-$ mass distributions. The calculated errors in these fitted masses amount to about 50 MeV for $M(\pi^-\pi^-\pi^+)$ and 15 MeV for $M(\pi^-\pi^+ p)$ in the regions of the diffractive peaks and justify the finely binned histograms in Figs. 6b and 7b. The shaded region in Fig. 6 is defined by the additional requirement that $|\Delta P_{T\varphi}| \leq 0.1$ GeV/c to reduce the background by about a factor of two.

The $M(\pi^-\pi^-\pi^+)$ spectrum in Fig. 6b is dominated by a very clear peak at about 1100 MeV, presumably due to the A_1. If there are higher mass 3π

diffractive states, they certainly do not become prominent at this energy. Similarly the $\pi^-\pi^+p$ state appears, within the somewhat meager statistics, to have a prominent peak at about 1550 MeV, close to the 1500 MeV peak which seems to dominate the $M(\pi^-\pi^+p)$ spectrum at much lower energies.

Figure 8ab show the t distributions for the π [$M(\pi^-\pi^-\pi^+) < 3$ GeV] and nucleon [$M(\pi^-\pi^+p) < 3.2$ GeV] diffractive peaks. The very peripheral nature of these events is quite evident and consistent with their interpretation as diffractive processes.

Figure 9 shows $\pi\pi$ mass spectra for pion diffraction events [$M(3\pi) < 3$ GeV] with the additional cut $|\Delta P_{T\varphi}| < 0.1$ GeV/c imposed to minimize background. In order to search for $\pi^+\pi^-$ resonances, we have made the assumption that the $\pi^-\pi^-$ mass spectrum is the same as that of $\pi^+\pi^-_b$ where π^-_b is the "bachelor" π^- and have subtracted it from the total $\pi^+\pi^-$ spectrum giving the residual distribution shown in Fig. 9c. This distribution appears to be dominated by the ρ peak with very little contribution from f, g or any higher mass mesons. If a significant contribution from reaction (3) is contained in the data, the peak in Fig. 4c could well represent a K^* state.

Figure 10 shows $p\pi^+$ and $p\pi^-$ mass spectra for the nucleon diffraction events [$M(\pi^-\pi^+p) < 3.2$ GeV]. A prominent Δ^{++} peak as well as some Δ^o are evident.

We complete this discussion by quoting our estimates of the pion dissociation and nucleon dissociation cross sections,

$$\sigma(\pi^- \rightarrow \pi^-\pi^-\pi^+) = 330\pm55\ \mu b\ ,$$
$$\sigma(p \rightarrow \pi^-\pi^+p) = 180\pm36\ \mu b\ .$$

For the $M(\pi\pi\pi)$ region 800-1200 MeV which includes the A_1 peak in Fig. 6b, the cross section is 160±40 μb. This number differs very little from the measured value in the same mass range at 20 GeV of 190±30 μb, further demonstrating the diffractive nature of the phenomenon.[3]

IV. DIFFRACTIVE PROCESSES LEADING TO NEUTRALS IN FINAL STATE

A. Pion Diffraction

Considering first 2-prong interactions, we show in Fig. 11a, the spectrum of M^2, the mass squared recoiling against the proton for events with slow identified protons in the final state which do not fit the elastic hypothesis. A large peak centered at $M^2 = 2$ GeV^2 of full width 4 GeV^2 is seen. Since the mass resolution is ± 1.5 GeV^2, we cannot say much about the detailed shape of the spectrum except that it evidently does not extend to very high masses. Indeed the spectrum is not inconsistent with what one expects from the $M(\pi^-\pi^-\pi^+)$ distribution shown in Fig. 6 and probably arises, in part, from A_1 production and decay via the $\pi^-\pi^o\pi^o$ mode. The t distribution for the events in the peak is shown in Fig. 11b and is highly peripheral as expected. Just as in elastic scattering, there is a loss of events at very low t, so that the first bin in the distribution is not reliable.

We have estimated the cross section for the pion diffractive dissociation,

$$\pi^- p \rightarrow (\pi^- + \text{neutrals}) + p$$

taking into account (i) that some of the inelastics may fit the elastic fit hypothesis, (ii) that some low t events are lost. Making no background subtraction under the mass peak in Fig. 11, and considering the diffraction region to extend to $M^2 = 20$ GeV^2 we obtain for the cross section

$$\sigma(\pi^- \rightarrow \pi^- + \text{neutrals}) = 700 \pm 100\ \mu\text{b} .$$

This value is significantly larger than the cross section for dissociation into $\pi^-\pi^-\pi^+$, namely 330 μb. It seems likely that the decay mode (π^- + neutrals) includes diffractive states with more than two π^o.

Similarly the spectrum of mass squared recoiling against identified protons in 4-prong processes with missing neutrals is shown in Fig. 12a,

with the t distribution for low mass events shown in Fig. 12b. A considerably broader enhancement at low M^2 is observed, extending to M^2 values of about 30 GeV^2. The estimate of the cross section for π^- dissociation into ($\pi^-\pi^-\pi^+$ + neutrals) is much less certain than for (π^- + neutrals) because of the small signal-to-background ratio. For the purposes of this analysis we simply neglect background and take as our measure the event population below $M^2 = 30$ GeV^2. Again, adding on the background included in the fits to reaction (2) and introducing a generous error to take account of the uncertainties due to the unsubtracted background we obtain

$$\sigma(\pi^- \rightarrow \pi^-\pi^-\pi^+ + \text{neutrals}) = 540\pm130\ \mu b \quad .$$

The cross section for pion dissociation into 2- and 4-prong events is then

$$\sigma[\pi^- \rightarrow \pi^*(2P,4P)] = 330 + 700 + 540 = 1.57\pm0.2\ mb \quad .$$

B. Nucleon Diffraction

Unfortunately the method used above to analyze the pion diffraction does not apply to the study of target dissociation. In order to obtain some information on this point we have attempted to separate in both two- and four-prong events the nucleon dissociations by using the following criteria.

(1) There must be a fast outgoing π^- of momentum within four standard deviations of 205 GeV/c.

(2) If there is an identified slow proton, the recoil mass squared must be greater than 30 GeV^2 (to eliminate pion dissociation background).

(3) The total energy of all visible tracks recoiling against the fast negative pion must be less than 15 GeV. This test helps eliminate background and is such as not to discriminate against nucleon dissociation into final states of mass squared less than 25 GeV^2.

In order to look for a highly peripheral contribution of events satisfying these tests we have plotted the angular deviation $\Delta\varphi$ in the plane perpendicular to the camera lens axis between the outgoing fast π^- and the beam particle, using an assumed momentum of 205 GeV/c to recalculate the direction of the outgoing pion. These plots for various classes of two-prong and four-prong events are shown in Figs. 13 and 14. These data all strongly populate the $\Delta\varphi$ region below 0.1 degree ($-t \lesssim 0.15$ GeV^2), and hence are in fact highly peripheral. Using $\Delta\varphi < 0.2^\circ$ as a definition of nucleon dissociation events, and making small corrections for inefficiencies in recognizing protons we obtain the following cross-section estimates,[4]

$$\sigma(p \rightarrow p + \text{neutrals}) = 220\pm40\ \mu b \ ,$$
$$\sigma(p \rightarrow \pi^+ + \text{neutrals}) = 420\pm70\ \mu b \ ,$$
$$\sigma(p \rightarrow p\pi^+\pi^- + \text{neutrals}) = 170\pm40\ \mu b \ ,$$
$$\sigma(p \rightarrow \pi^+\pi^+\pi^- + \text{neutrals}) = 440\pm130\ \mu b \ ,$$
$$\sigma(p \rightarrow p\pi^+\pi^-) = 180\pm36\ \mu b \ .$$

Thus the cross section for proton dissociation into 2- and 4-prong events is,

$$\sigma[p \rightarrow p^*(2P,4P)] = 1.43\pm0.2\ \text{mb} \ .$$

C. Discussion

It should be first emphasized that the diffraction cross sections quoted are obtained by simple counting procedures with no background subtraction. We have assigned generous errors which we believe should encompass whatever modifications a more sophisticated treatment would bring. With this qualification, we can indicate some interesting features:

(i) The ratio between the dissociation cross sections $\sigma(p \rightarrow p + \text{neutrals})$ and $\sigma(p \rightarrow \pi^+ + \text{neutrals})$, namely $(220\pm40)/(420\pm70)$, is in good agreement with the value $1/2$ expected if the dominant final states involve just a nucleon plus a single pion in an $I = 1/2$ state.

(ii) The total two-prong pion and proton dissociation cross sections, namely 700±100 and 640±80 μb respectively, are about the same size. The total four-prong dissociation cross sections, namely 870±140 μb and 790±140 μb, similarly are nearly equal. It appears on the basis of these comparisons, that there may be near equality between the pion and proton dissociation cross sections for each individual multiplicity. If we assume this to hold at higher multiplicities as well, we may speculate that,

$$\sigma(\pi \rightarrow \pi^*) = \sigma(p \rightarrow p^*) \quad ,$$

where π^*, p^* represent the totality of all states produced by the dissociation of pions and protons. Assuming factorizable Pomeron exchange to account for these diffraction dissociation processes, one would then obtain the following relation,

$$\frac{g^2(P\pi\pi)}{g^2(P\pi\pi^*)} = \frac{g^2(Ppp)}{g^2(Ppp^*)} \quad ,$$

where the g's are the appropriate coupling constants. One consequence of this relation which can be submitted to experimental test by suitable comparison with proton-proton interaction data is the following prediction,

$$\left.\frac{\sigma(p \rightarrow p^*)}{\sigma(p \rightarrow p)}\right|_{pp \text{ collisions}} = \left.\frac{\sigma(\pi \rightarrow \pi^*)}{\sigma(\pi \rightarrow \pi)}\right|_{\pi p \text{ collisions}}$$

where the cross sections in the denominators are just the elastic pp and πp cross sections.[5]

(iii) Finally it is interesting to note that diffraction processes (elastic and inelastic) account for 90% of all 2-prong events and 50% of all 4-prong events. They clearly dominate the low multiplicities.

We want to express our gratitude to the 30-inch bubble chamber staff, the hadron beam group, the accelerator operations personnel, and our scanning and measuring staffs for their outstanding efforts.

FOOTNOTES AND REFERENCES

*Work supported in part by the U. S. Atomic Energy Commission, the National Science Foundation, and C.N.R.S.

†Permanent address: Laboratoire de l'Accélérateur Linéaire, C.N.R.S., Orsay, France.

1. As discussed in Sec. II, this cross section may include a major contribution from reaction (3).

2. J. H. Boyd et al., Phys. Rev. 166, 1458 (1968);
S. U. Chung et al., Phys. Rev. 165, 1491 (1968);
J. W. Lamsa et al., Phys. Rev. 166, 1395 (1968);
C. Caso et al., Nuovo Cimento 57A, 699 (1968);
M. L. Ioffredo et al., Phys. Rev. Letters 21, 1212 (1968);
J. Ballam et al., Phys. Rev. Letters 21, 934 (1968).

3. D. Chew et al., Search for Pomeron-Pomeron-2π Events in 205 GeV/c $\pi^- p$ Interactions, Abstract submitted to the APS Division of Particles and Fields Meeting, Berkeley, August 13-17, 1973; LBL-2106 Abstract.

4. In referring to the presence or absence of a proton, we have assumed here that the protons will be slow and hence recognizable. It is quite possible that in some of the baryon dissociation processes, a proton of momentum above 1.5 GeV/c is emitted and hence the event is classified as a dissociation of the form $p \rightarrow \pi$ + neutrals or $p \rightarrow 3\pi$ + neutrals.

5. The cross section $\sigma(p \rightarrow p^*)$ corresponds to a single vertex and is therefore half of the total p-p single diffractive dissociation cross section.

FIGURE CAPTIONS

Fig. 1. Plot of M_R^2 vs $\Delta P_{T\varphi}$ for 2-prong events; (a) no restriction other than fiducial volume and track length; (b) elastic fit with $\chi^2 < 30$ also required.

Fig. 2. Plot of M_R^2 vs $\Delta P_{T\varphi}$ for 4-prong pion diffraction events [$M^2(\pi^-\pi^-\pi^+) < 20$ GeV^2]; (a) no restriction other than fiducial volume and track length; (b) fit to $\pi^-\pi^-\pi^+p$ with $\chi^2 < 30$ also required.

Fig. 3. Plot of M_R^2 vs $\Delta P_{T\varphi}$ for 4-prong nucleon diffraction events [$M^2(\pi^-\pi^-\pi^+) > 20$ GeV^2]; (a) no restriction other than fiducial volume and track length; (b) fit to $\pi^-\pi^-\pi^+p$ with $\chi^2 < 30$ also required.

Fig. 4. Momentum dependence of $\pi^-\pi^-\pi^+p$ cross section.

Fig. 5. Plot of $M^2(\pi^-\pi^-\pi^+)$ vs the lower value of $M^2(\pi^-\pi^+p)$.

Fig. 6. $M(\pi^-\pi^-\pi^+)$ distribution; (a) 200 MeV bins; (b) 50 MeV bins.

Fig. 7. $M(\pi^-\pi^+p)$ distribution; (a) 200 MeV bins; (b) 50 MeV bins.

Fig. 8. t distributions; (a) π dissociation [$M(\pi^-\pi^-\pi^+) < 3$ GeV]; (b) nucleon dissociation [$M(\pi^-\pi^+p) < 3.2$ GeV].

Fig. 9. $M(\pi\pi)$ spectra for pion dissociation [$M(\pi^-\pi^-\pi^+) < 3$ GeV]; (a) $M(\pi^+\pi^-)$--two entries per event, (b) $M(\pi^-\pi^-)$--one entry per event, (c) difference of (a) and (b)--one entry per event.

Fig. 10. $M(\pi p)$ spectra for nucleon dissociation [$M(\pi^-\pi^+p) < 3.2$ GeV]; (a) $M(\pi^+p)$, (b) $M(\pi^-p)$.

Fig. 11. (a) Spectrum of M^2, the mass squared recoiling against the proton for 2-prong inelastic events with identified slow protons; (b) t distribution for those events with $M^2 < 10$ GeV^2.

Fig. 12. (a) Spectrum of M^2, the mass squared recoiling against the proton for 4-prong events with missing neutrals and identified slow protons; (b) t distribution for those events with $M^2 < 20$ GeV^2.

Fig. 13. Distribution of Δp for events selected as described in text. (a) 2-prong inelastic events with identified slow proton; (b) 2-prong inelastic events without identified slow proton.

Fig. 14. Distribution of Δp for events selected as described in text. (a) 4-prong events which fit reaction (2); (b) 4-prong events which do not fit reaction (2) and have an identified slow proton; (c) 4-prong events which do not fit reaction (2) and do not have an identified slow proton.

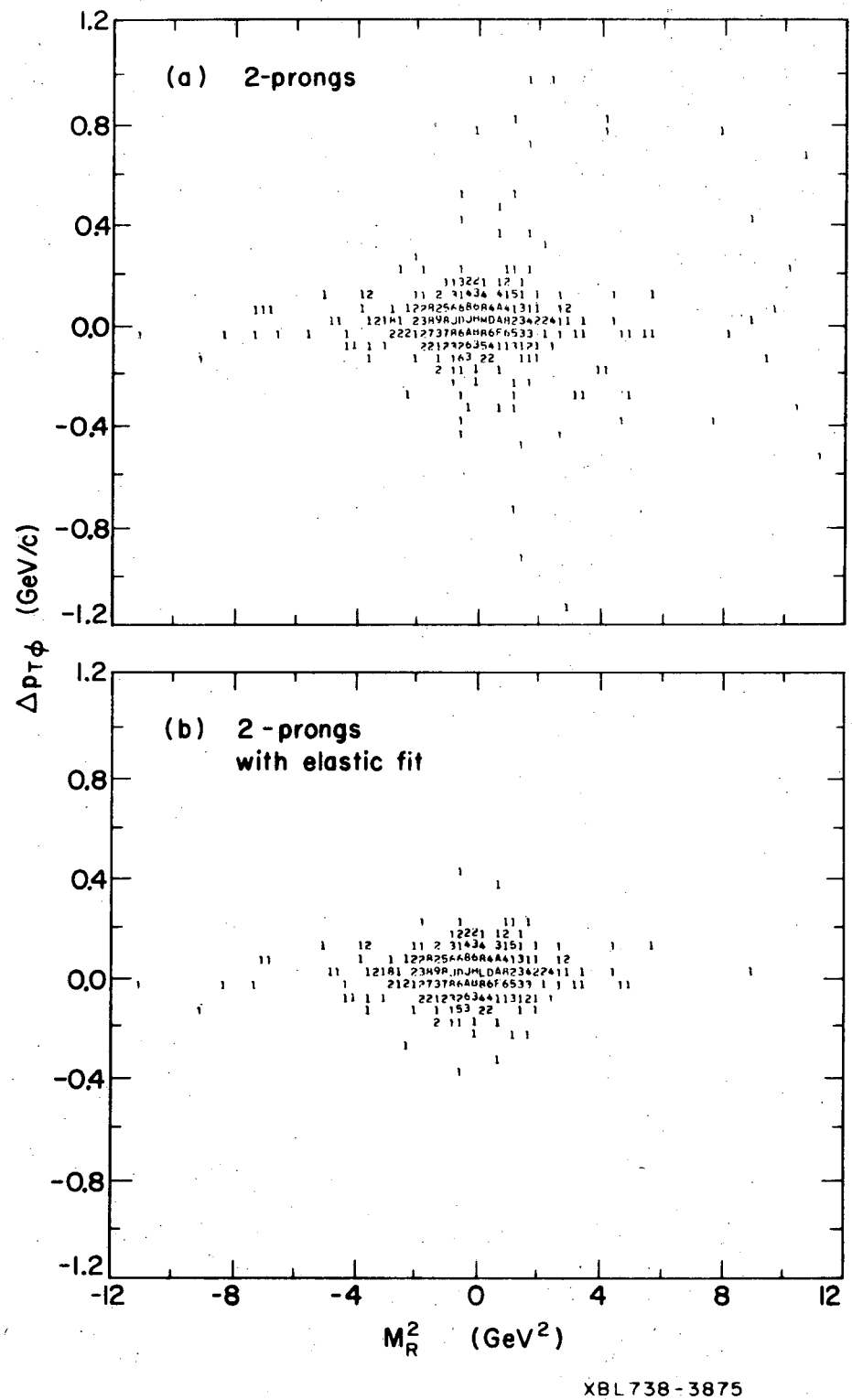
(a) 2-prongs
(b) 2-prongs
with elastic fit
$\Delta p_T \phi$ (GeV/c)
M_R^2 (GeV^2)
1.2
0.8
0.4
0.0
-0.4
-0.8
-1.2
-12
-8
-4
0
4
8
12
XBL738-3875

Fig. 1

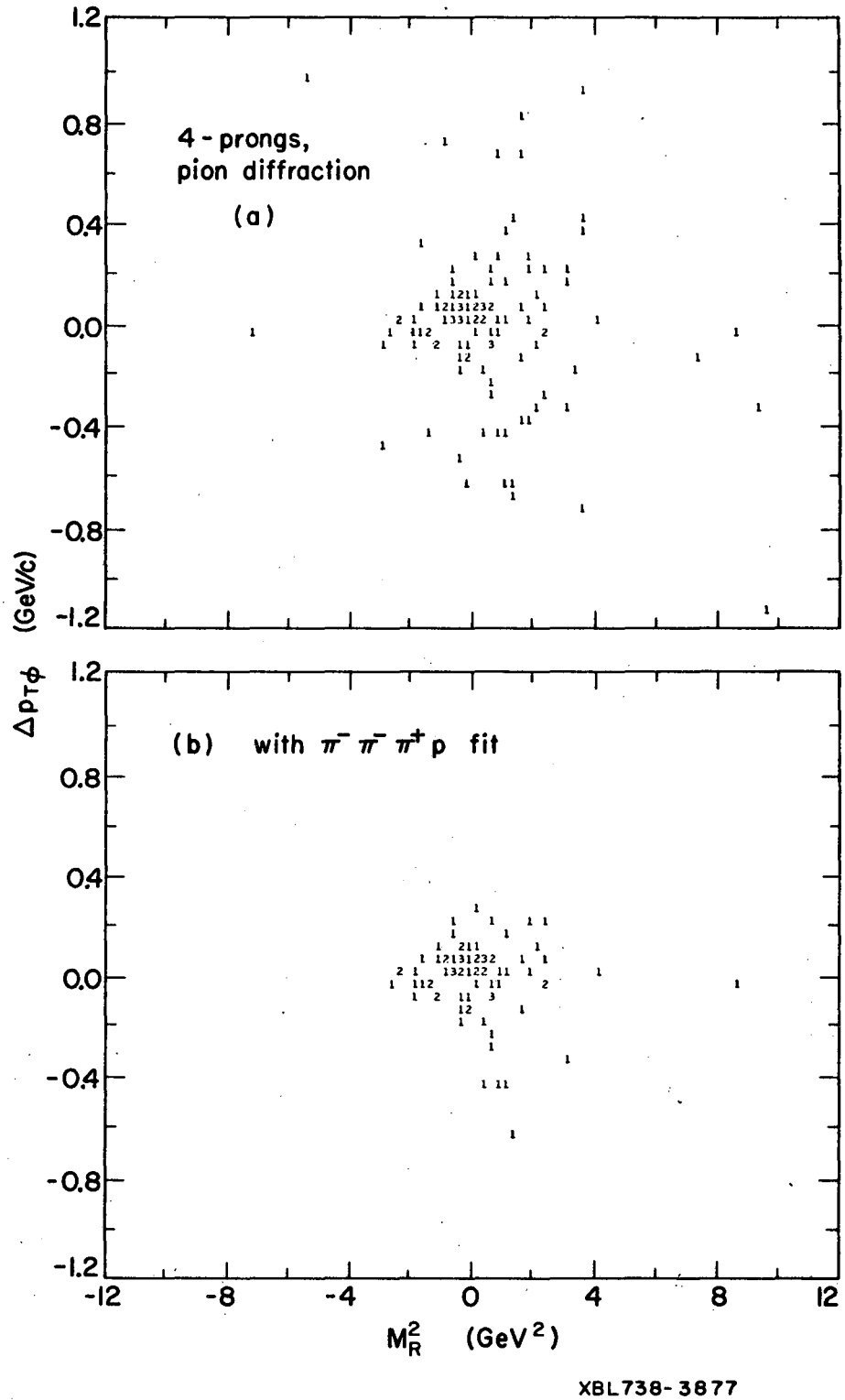
4 - prongs,
pion diffraction
(a)
(b) with $\pi^-\pi^-\pi^+$ p fit
$\Delta p_{T\phi}$ (GeV/c)
1.2
0.8
0.4
0.0
-0.4
-0.8
-1.2
-12
-8
-4
0
4
8
12
M_R^2 (GeV^2)
XBL738-3877

Fig. 2

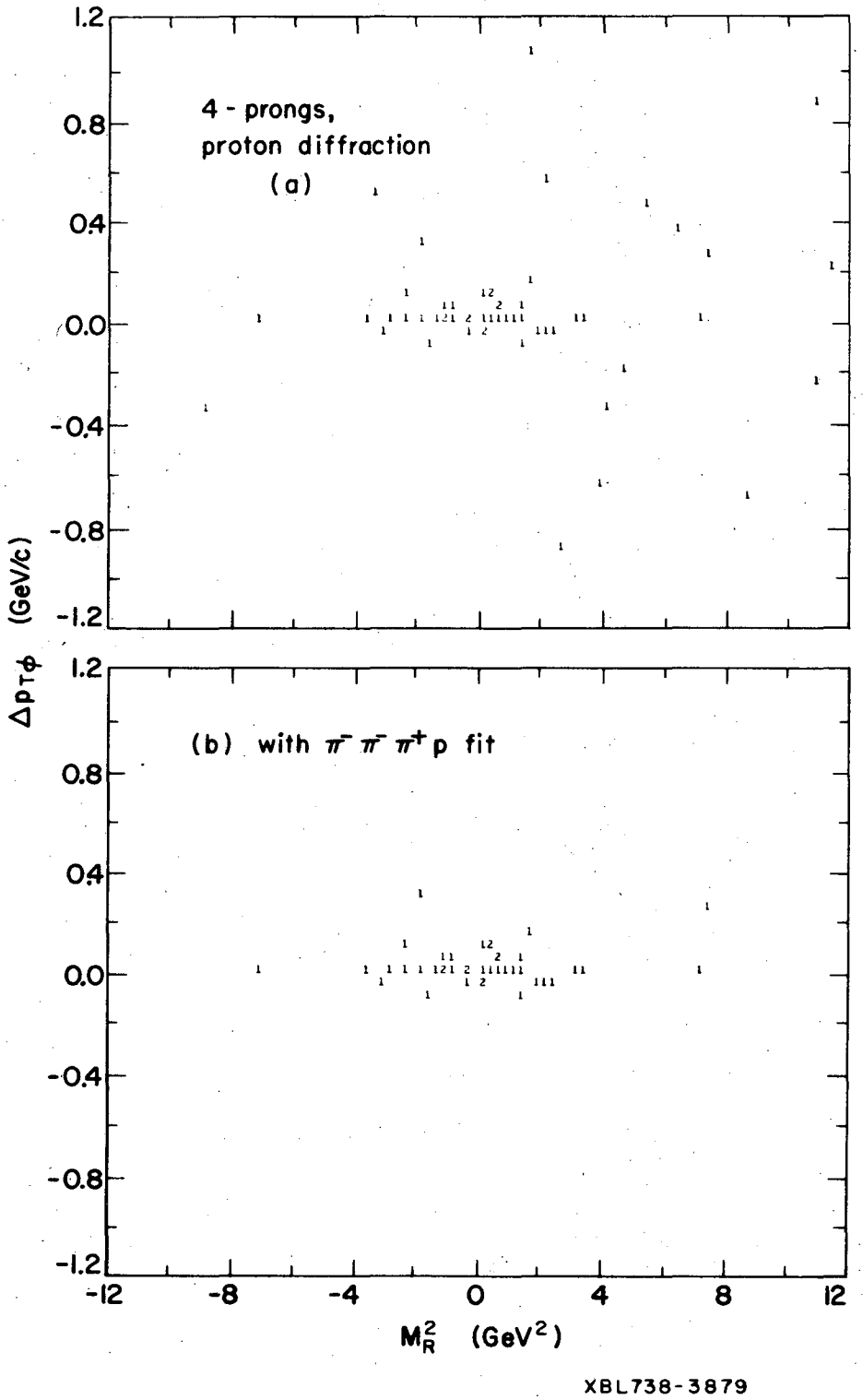
4 - prongs,
proton diffraction
(a)
(b) with $\pi^-\pi^-\pi^+$ p fit
$\Delta p_T \phi$ (GeV/c)
1.2
0.8
0.4
0.0
-0.4
-0.8
-1.2
-12
-8
-4
0
4
8
12
M_R^2 (GeV^2)
XBL738-3879

Fig. 3

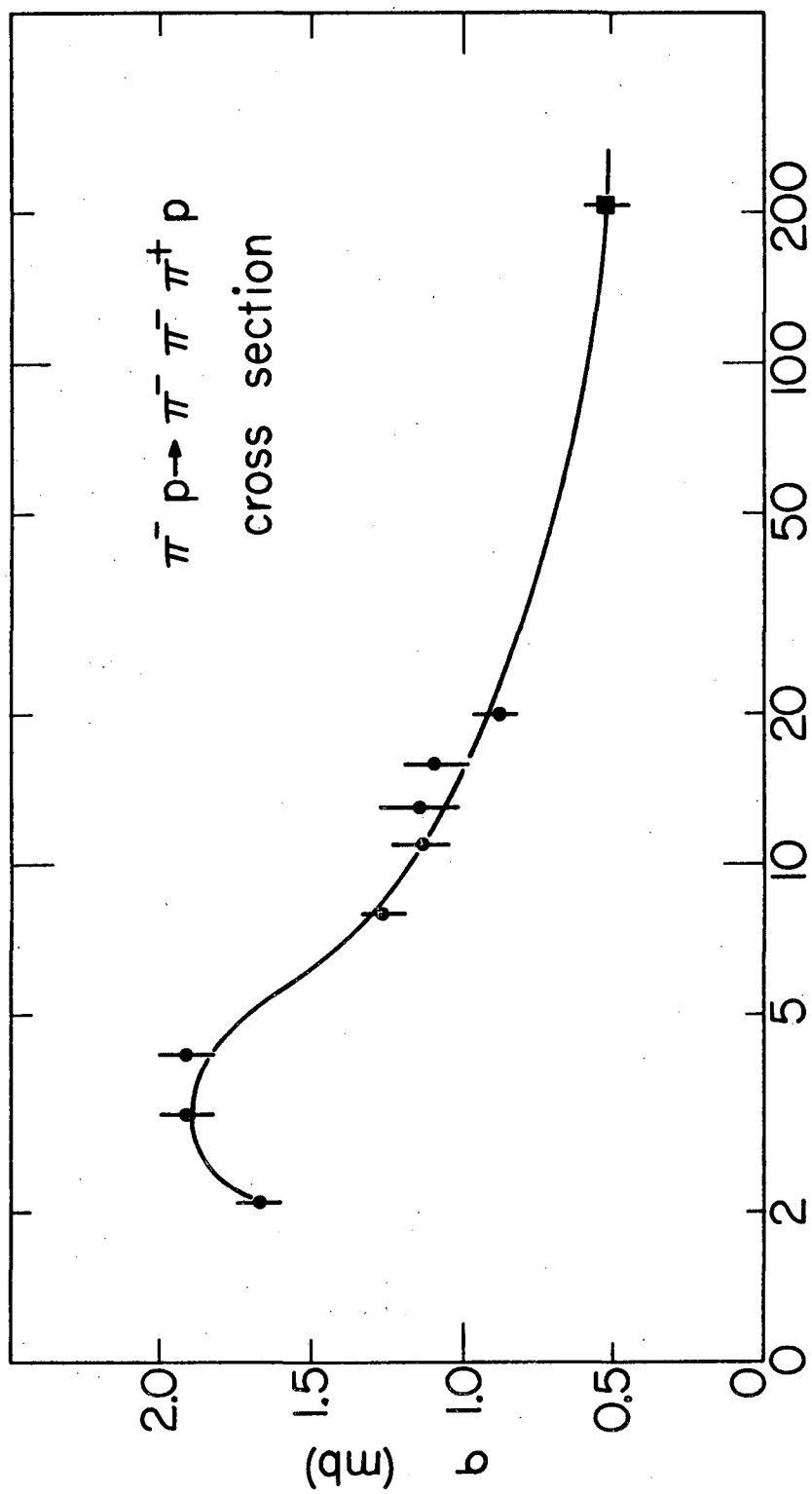
$\pi^- p \rightarrow \pi^- \pi^- \pi^+ p$
cross section
σ (mb)
2.0
1.5
1.0
0.5
0
0
2
5
10
20
50
100
200
π^- momentum (GeV/c)
XBL738-3880

Fig. 4

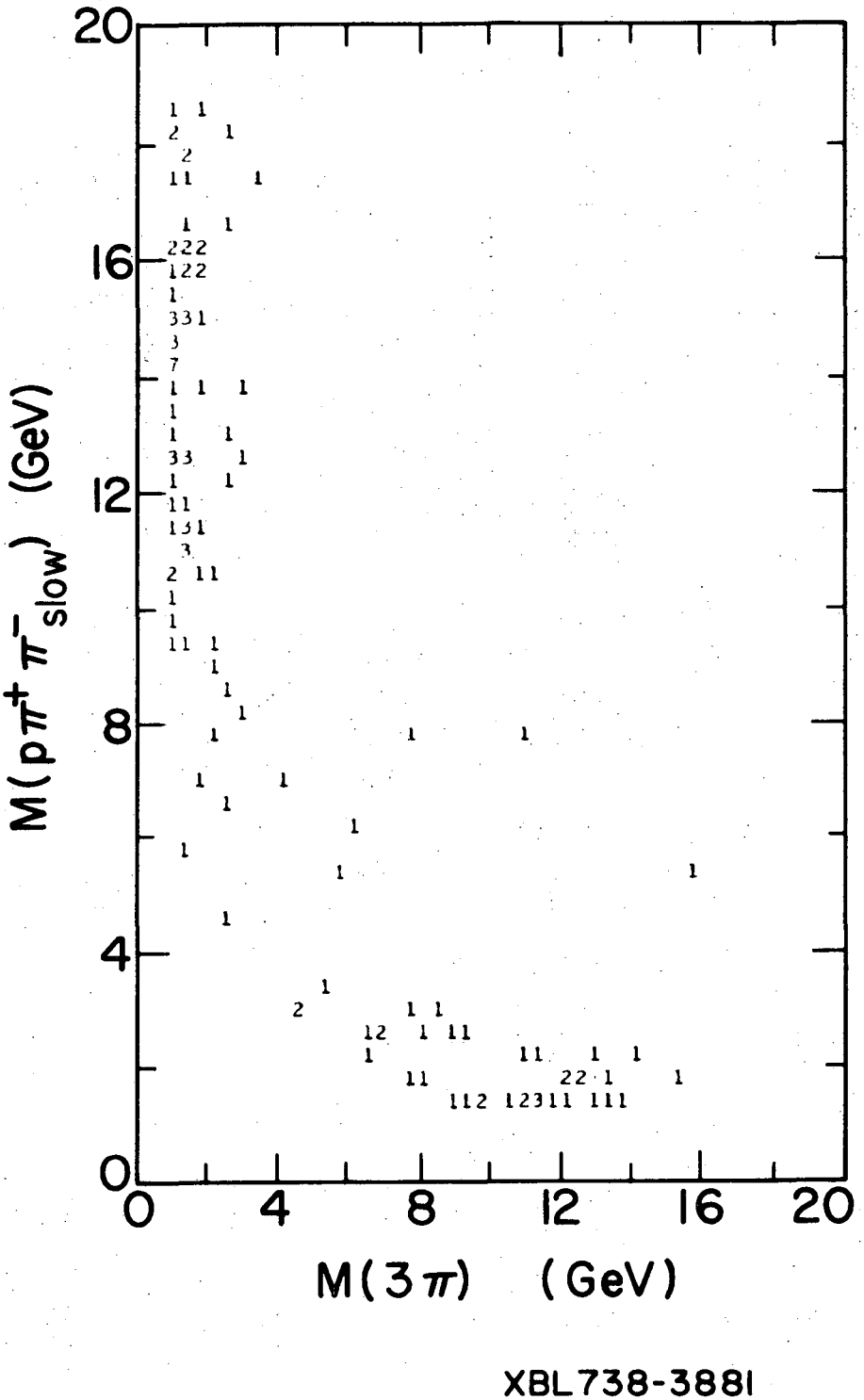

Fig. 5

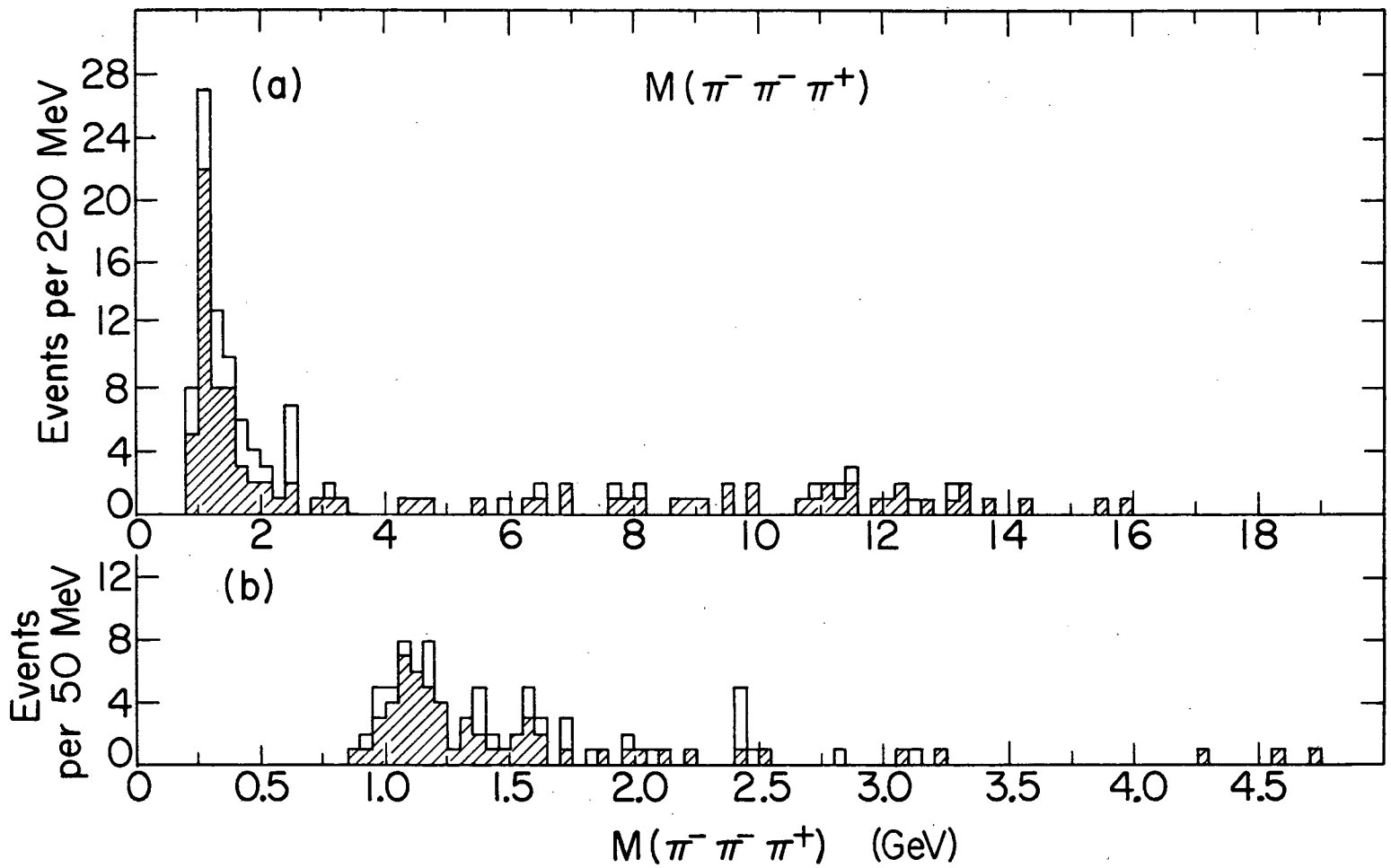

XBL738-3882

Fig. 6

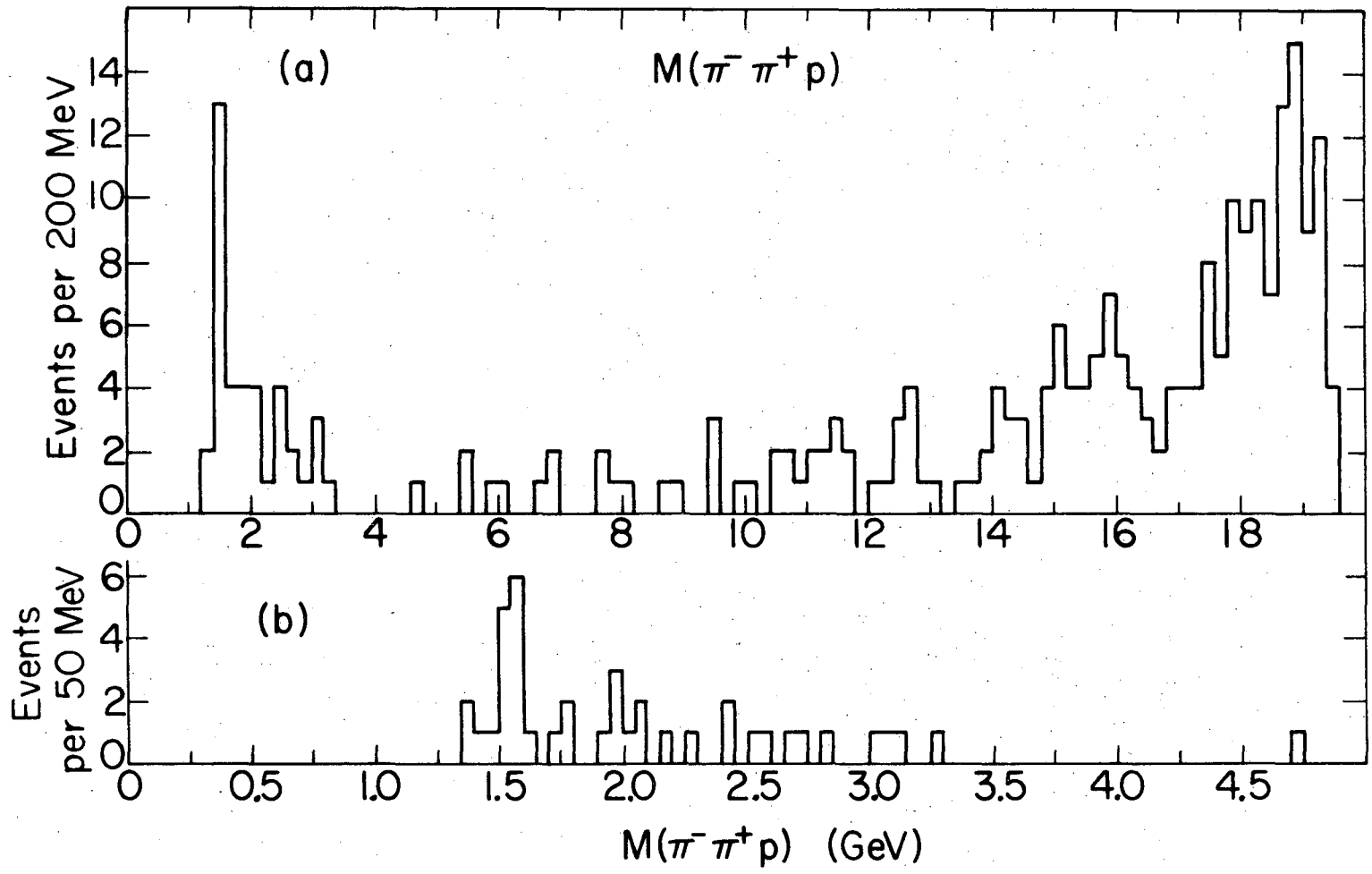
(a)
M(π⁻ π⁺ p)
Events per 200 MeV
0
2
4
6
8
10
12
14
16
18
(b)
Events per 50 MeV
0
0.5
1.0
1.5
2.0
2.5
3.0
3.5
4.0
4.5
M(π⁻ π⁺ p) (GeV)
XBL738-3883

Fig. 7

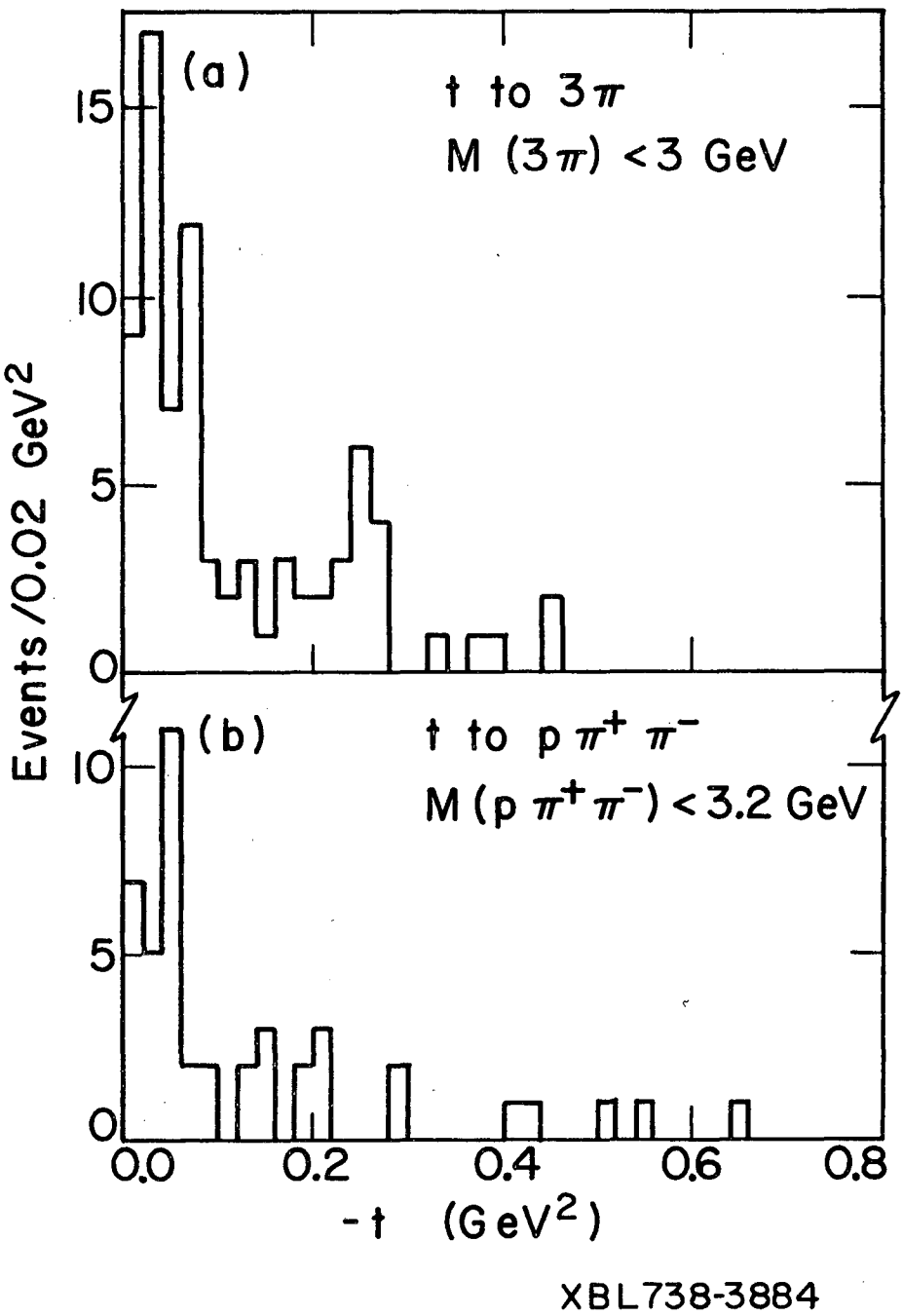
(a)
t to 3π
M (3π) <3 GeV
15
10
5
0
(b)
t to p π+ π−
M (p π+ π−) <3.2 GeV
10
5
0
Events /0.02 GeV2
0.0
0.2
0.4
0.6
0.8
-t (GeV2)
XBL738-3884

Fig. 8

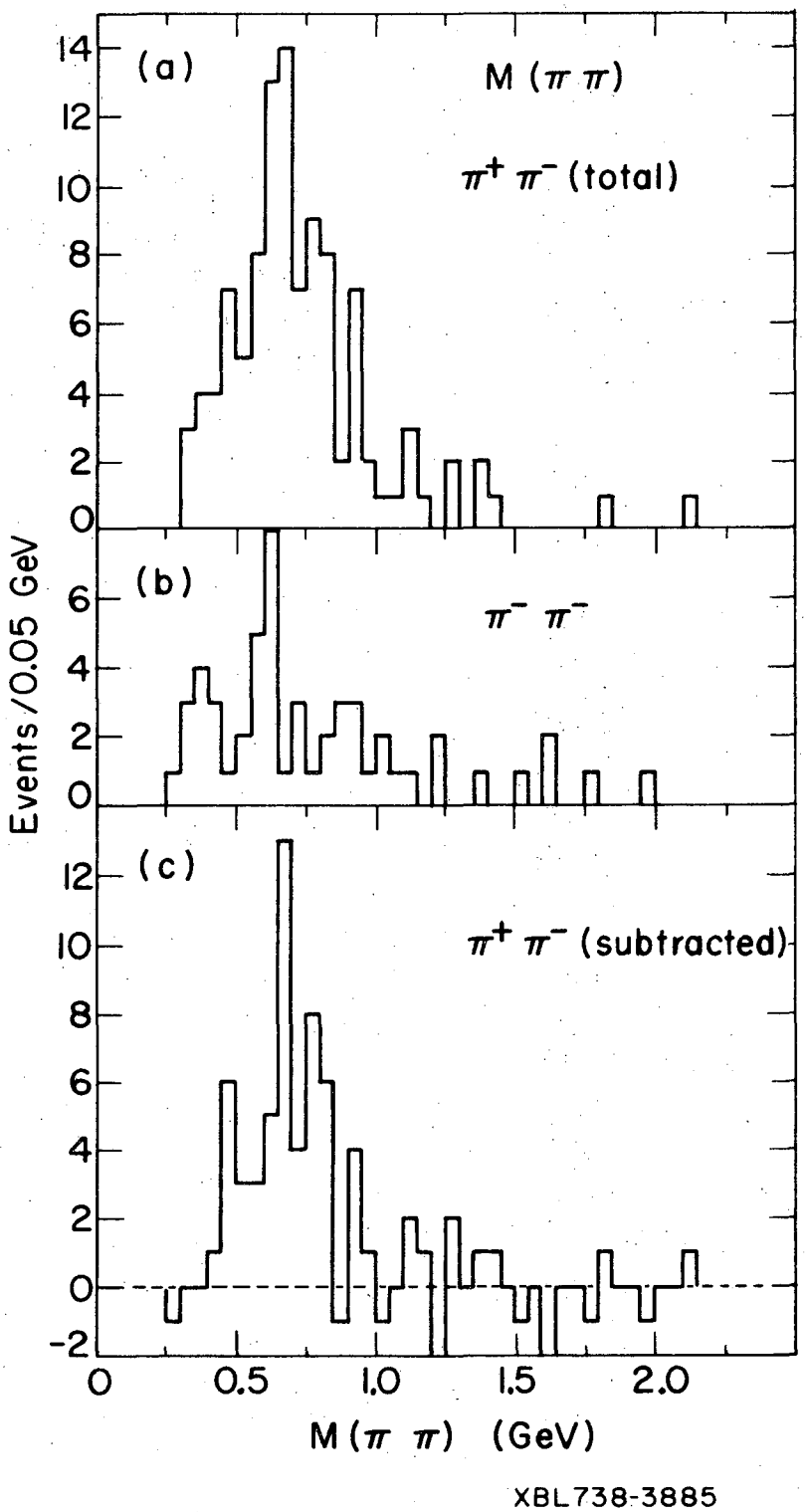
(a)
M (π π)
π+ π− (total)
(b)
π− π−
(c)
π+ π− (subtracted)
Events/0.05 GeV
M (π π) (GeV)
XBL738-3885

Fig. 9

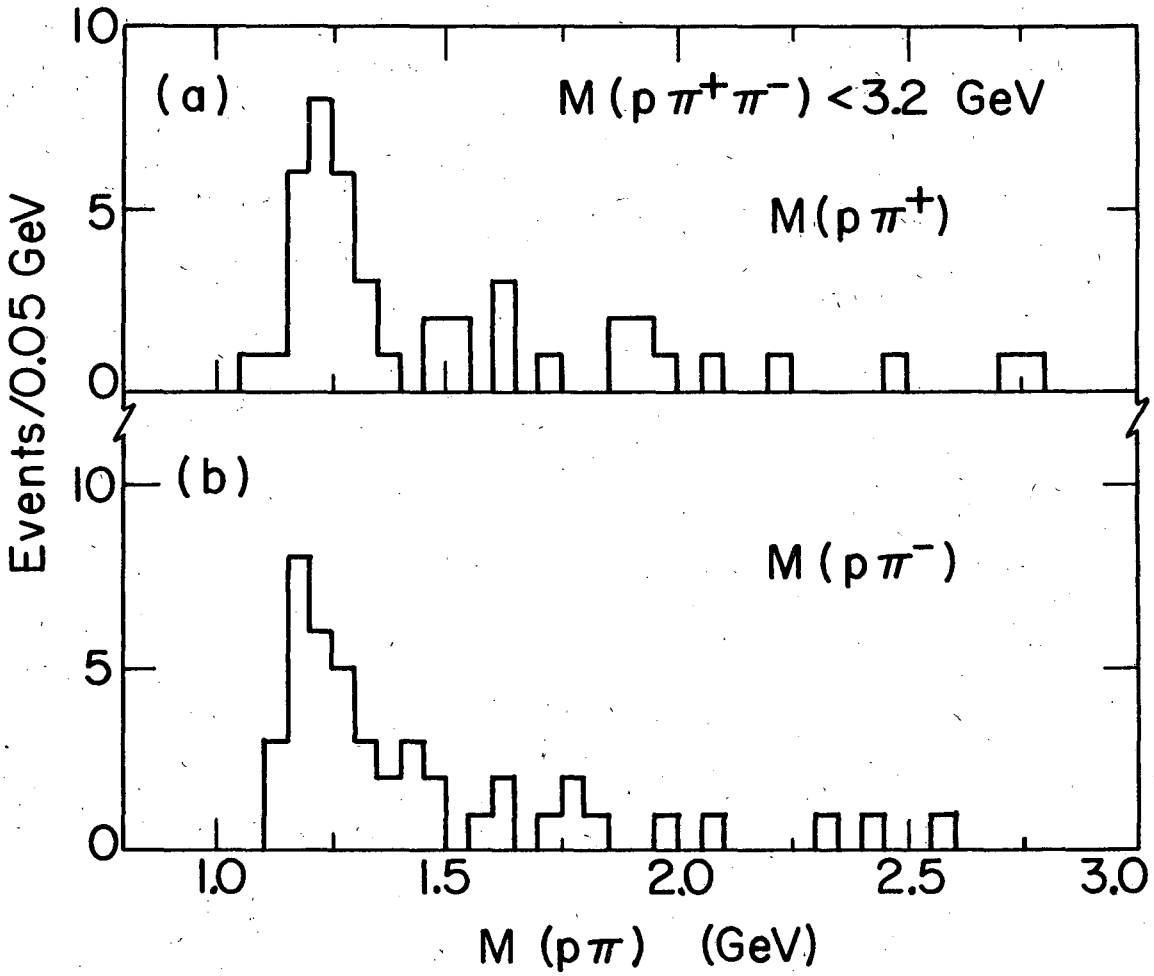
(a)
M(pπ+π−) <3.2 GeV
M(pπ+)
(b)
M(pπ−)
Events/0.05 GeV
10
5
0
1.0
1.5
2.0
2.5
3.0
M (pπ) (GeV)
XBL738-3886

Fig. 10

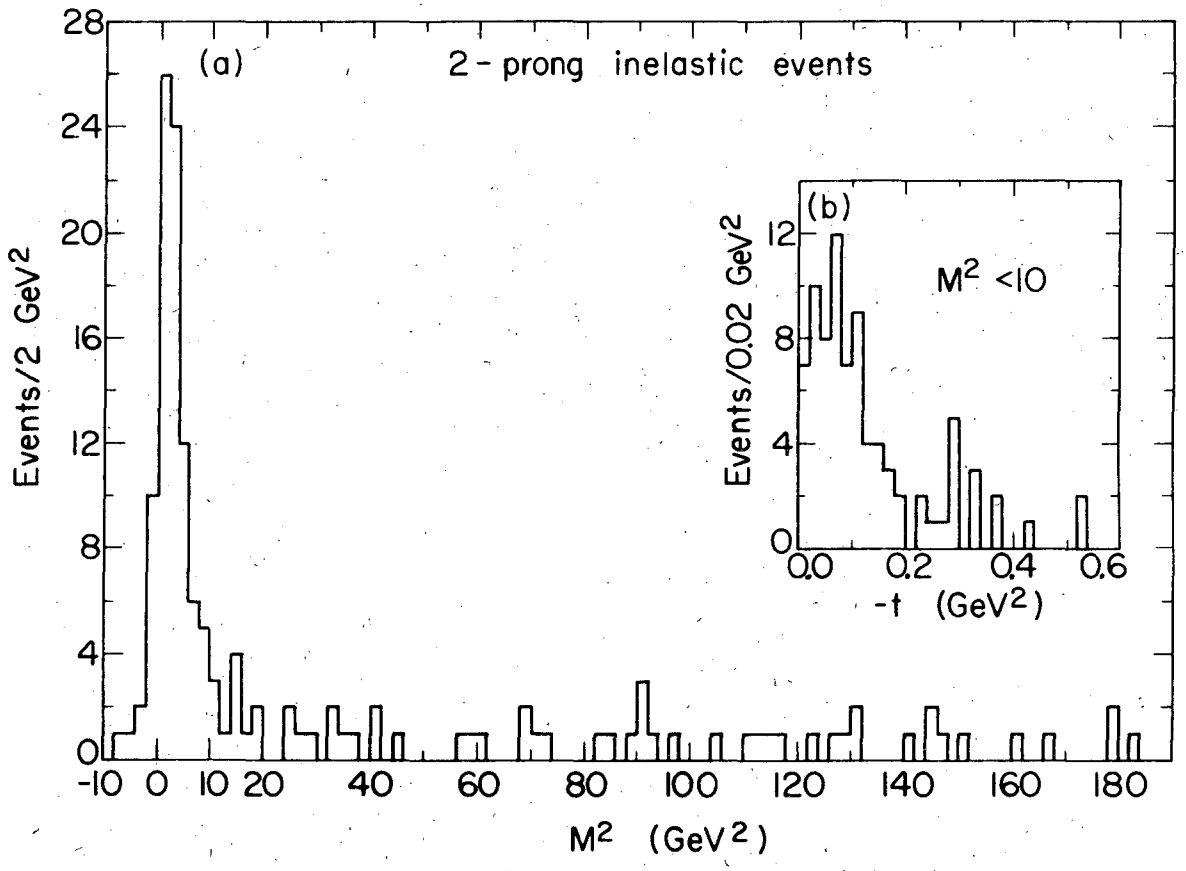
(a)
2 - prong inelastic events
Events/2 GeV²
M² (GeV²)
(b)
M² <10
Events/0.02 GeV²
-t (GeV²)
XBL 738-3887

Fig. 11

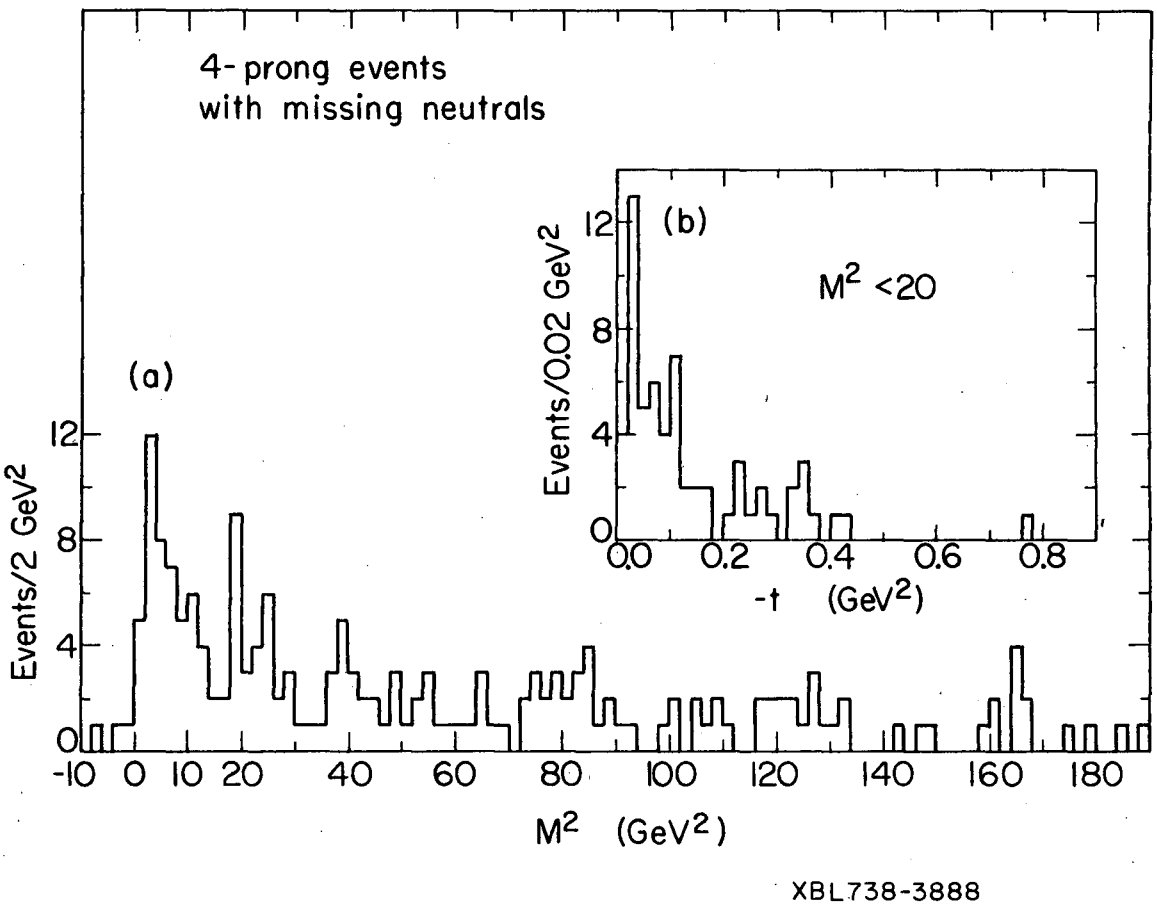
4-prong events
with missing neutrals
(a)
(b)
M^2 <20
Events/2 GeV^2
Events/0.02 GeV^2
M^2 (GeV^2)
-t (GeV^2)
XBL738-3888

Fig. 12

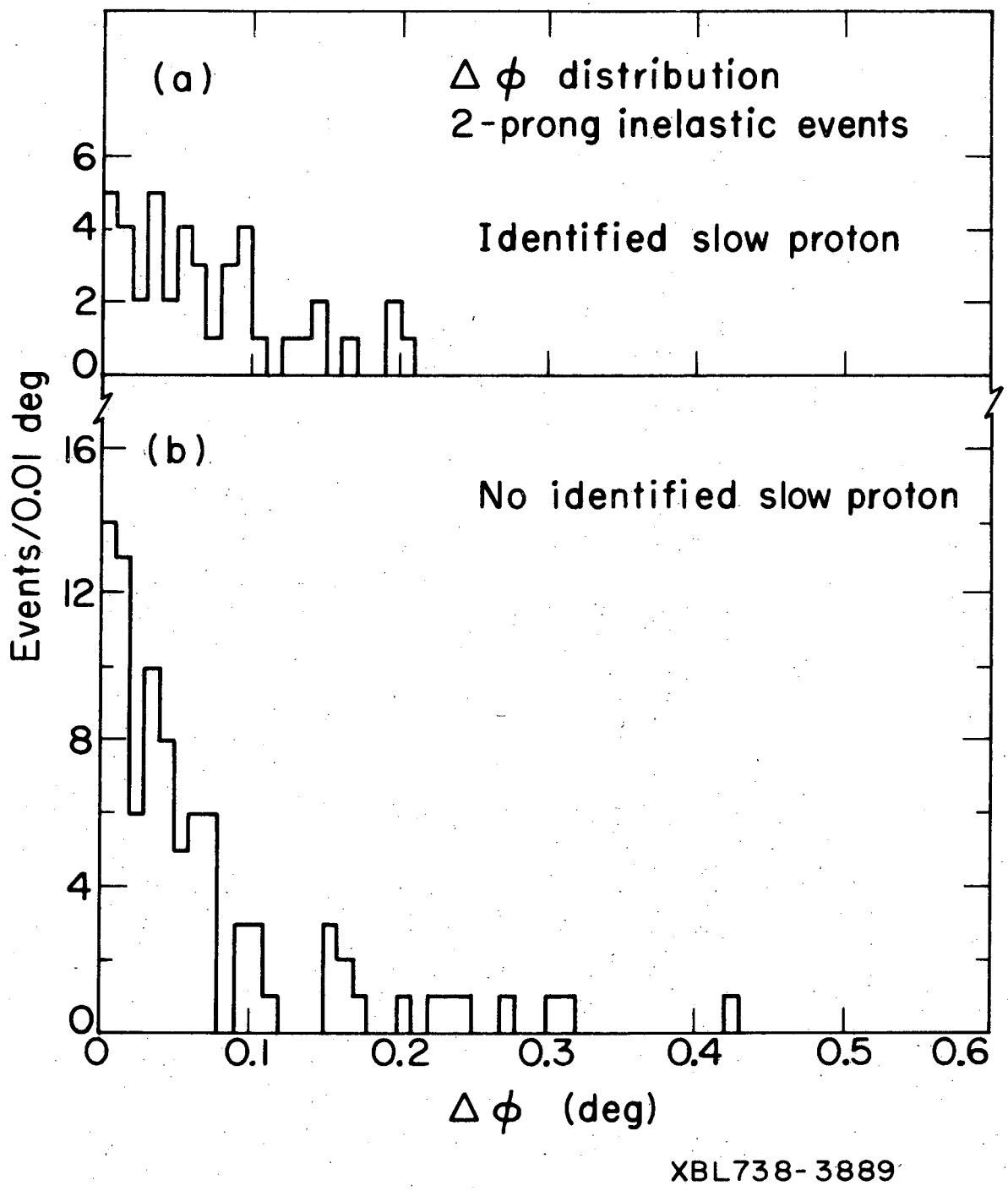
(a)
Δφ distribution
2-prong inelastic events
Identified slow proton
(b)
No identified slow proton
Events/0.01 deg
Δφ (deg)
0
2
4
6
8
12
16
0.1
0.2
0.3
0.4
0.5
0.6
XBL738-3889

Fig. 13

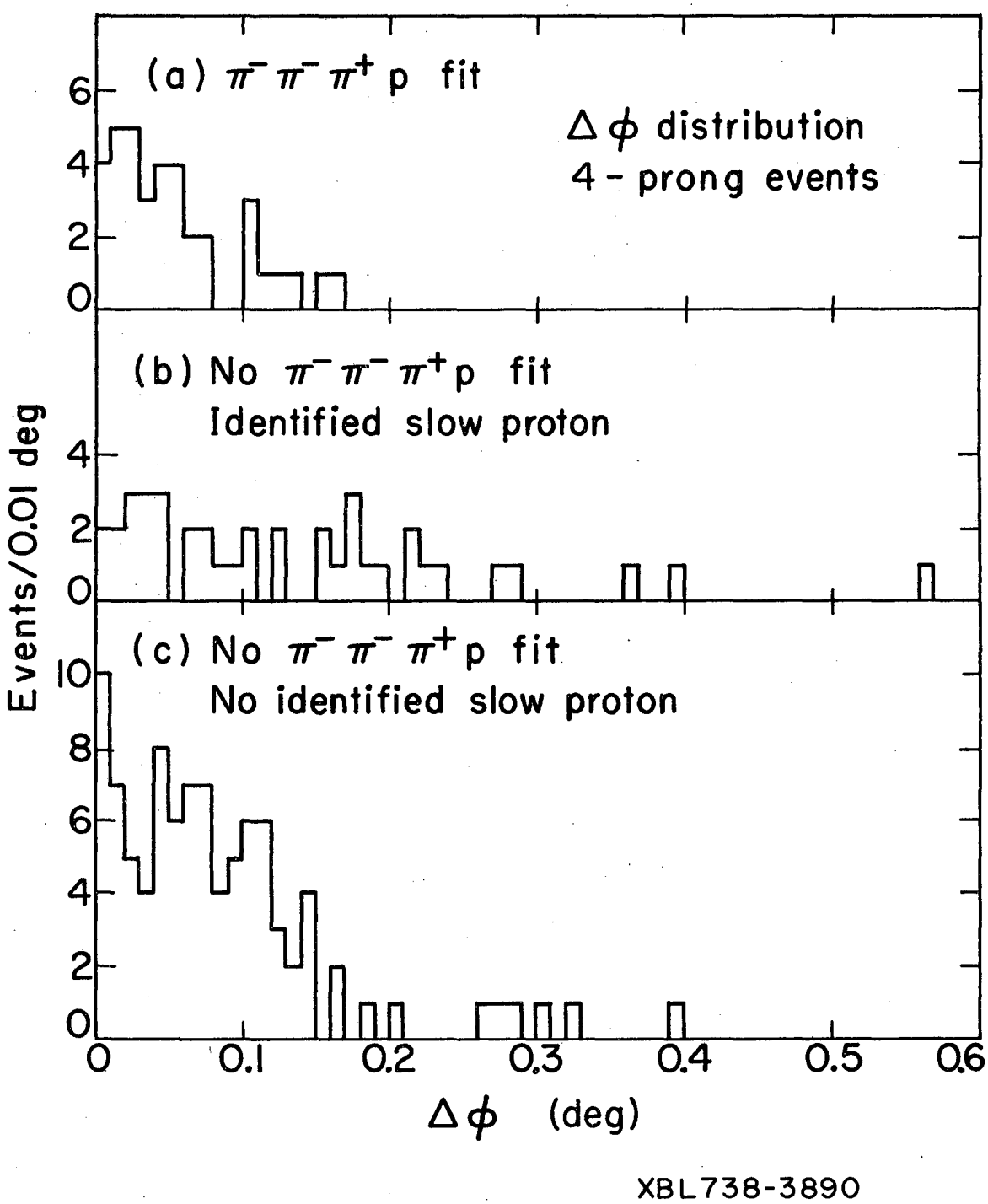
(a) $\pi^-\pi^-\pi^+$ p fit
$\Delta\phi$ distribution
4 - prong events
(b) No $\pi^-\pi^-\pi^+$ p fit
Identified slow proton
(c) No $\pi^-\pi^-\pi^+$ p fit
No identified slow proton
Events/0.01 deg
$\Delta\phi$ (deg)
0
0.1
0.2
0.3
0.4
0.5
0.6
XBL738-3890

Fig. 14

TECHNICAL INFORMATION DIVISION
LAWRENCE BERKELEY LABORATORY
UNIVERSITY OF CALIFORNIA
BERKELEY, CALIFORNIA 94720